Available online at www.sciencedirect.com
ScienceDirect
International Journal of Heat and Mass Transfer 51 (2008) 2006–2019
International Journal of HEAT and MASS TRANSFER
www.elsevier.com/locate/ijhmt

Reactants flow behavior and water management for different current densities in PEMFC

Dewan Hasan Ahmed, Hyung Jin Sung *, Joongmyeon Bae, Dong-Ryul Lee

Department of Mechanical Engineering, Korea Advanced Institute of Science and Technology, 373-1, Guseong-dong Yuseong-gu, Daejeon 305-701, Republic of Korea

Received 10 January 2006; received in revised form 9 April 2007
Available online 24 October 2007

Abstract

Computational fluid dynamics analysis was carried out to investigate the reactants flow behavior and water management for proton exchange membrane fuel cell (PEMFC). A complete three-dimensional model was chosen for single straight channel geometry considering both anode and cathode humidification. Phase transformation was included in the model to predict the water vapor and liquid water distributions and the overall performance of the cell for different current densities. The simulated results showed that for fully humidified conditions hydrogen mole fraction increases along the anode channel with increasing current density, however, at higher current densities it decreases monotonically. Different anode and cathode humidified conditions results showed that the cell performance was sufficiently influenced by anode humidification. The reactants and water distribution and membrane conductivity in the cell depended on anode humidification and the related water management. The cathode channel–GDL (Gas Diffusion Layer) interface experiences higher temperature and reduces the liquid water formation at the cathode channel. Indeed, at higher current densities the water accumulated in the shoulder area and exposed higher local current density than the channel area. Higher anode with lower cathode humidified combination showed that the cell had best performance based on water and thermal management and caused higher velocity in the cathode channel. The model was validated through the available literature.

1. Introduction

Proton Exchange Membrane Fuel Cell (PEMFC) is a strong candidate for future automobile and power generation because of its high power density, low emission and low operating temperature. Even though PEMFC has splendid advantages, it has some limitations especially at low and high current densities (CDs). Usually, at low current densities, the cell loses the voltage mainly due to the activation losses. At high current densities, the PEMFC loses the voltage as the reactants are depleted at the end of channels, which is called as concentration losses. Another kind of loss is ohmic losses – are mainly due to the electrical resistance of PEM (Proton Exchange Membrane) and bipolar plates. On top of the above losses, water management is the major issue of PEMFC's overall performance in different operating conditions. Indeed, water in the PEMFC itself has duel nature and has both advantages and disadvantages. PEM has higher proton conductivity at water saturation level and however, too much water in PEMFC causes further concentration losses. The produced water by the chemical reaction has significant effect on further reactant consumption and water management and the consequence of this causes dehydration or flooding in PEMFC. Computational fluid dynamics (CFD) technique can be used to determine the reactants flow behavior and water transportation for PEMFC.

More than a decade, many researches have been carried out for the basic understanding of water and thermal management and for the improvement of overall PEMFC performance. In recent years, numerical simulation

* Corresponding author. Tel.: +82 42 869 3027; fax: +82 42 869 5027.
E-mail address: hjsung@kaist.ac.kr (H.J. Sung).

0017-9310/$ - see front matter © 2007 Elsevier Ltd. All rights reserved.
doi:10.1016/j.ijheatmasstransfer.2007.06.027

Nomenclature

A_{cv}	specific surface area of the control volume, m^{-1}
C_{wa}	concentration of water vapor at anode, mol/m^3
C_{wc}	concentration of water vapor at cathode, mol/m^3
D_w	diffusion coefficient of water, m^2/s
F	Faraday constant, 96,487 C/mole
h_{rxn}	enthalpy of water formation, kJ/kmol
h_{fg}	enthalpy of vaporization of water, kJ/kg
I	local current density, A/m^2
$I_{o,K}$	exchange current density for reaction K, A/m^2
L	length, m
$M_{m,dry}$	equivalent weight of a dry membrane, kg/mole
M_n	molecular weight of species n, kg/mole
$mass_n$	mass of species n, kg
n_d	electro-osmosis drag coefficient
$P^{sat}_{w,k}$	saturation vapor pressure of water in stream K, Pa
P	pressure, Pa
P_n	partial pressure of species n, Pa
R	universal gas constant, 8.314 J/mol K
r	condensation rate, 1/s
S	source term
t_m	membrane thickness, m
T	temperature, K
V_{oc}	open circuit voltage, V
V_{cell}	cell voltage, V

Greek symbols

α	net water flux per proton
β	permeability, m^2
η	overpotential, V
λ	water content in the membrane
μ	dynamic viscosity, kg s/m^2
$\rho_{m,dry}$	density of a dry membrane, kg/m^3
ρ	density of the mixture, kg/m^3
σ_m	membrane conductivity, S/m

Subscripts and superscripts

a	anode
c	cathode
cv	control volume
e	electrochemical reaction
H_2	hydrogen
K	anode or cathode
l	liquid
O_2	oxygen
v	vapor
sat	saturated
ξ	dummy variable for direction x, y or z

techniques have been used for different aspects of PEMFC for the single channel and also for the different serpentine flow fields [1–15] to improve the cell performance. It is believed that the reactants distribution is one of the prime factors to enhance the cell performance. Different geometrical modifications have been also investigated in recent years in this aspect to achieve effective reactants distribution to the reacting area such as varying flow field (e.g., using serpentine, integrated flow field) [14,16], different channel–shoulder width combination [17,18], introducing baffles in the channel area [19], using converging channel cross-section [20], and deflected membrane [21]. However, it is important to know how the reactants' distributions in the fuel cell vary and depend on water management, current density and also with external humidification conditions. The reactants (hydrogen and oxygen) consumption in PEMFC depends on the current densities, the formation and transportation of water in the cell. Each H_2 ion (H^+) carries higher number of water molecules from anode to cathode by electro-osmosis drag and it causes the anode dehydration. However, at the cathode, H_2 ion reacts with O_2 through various reaction steps (like: adsorption step, rate-determining step and rapid step) and produces water, which causes the flooding problem in the cathode channel. Details of reaction pathway of oxygen reduction reaction (ORR) at cathode catalyst layer can be found elsewhere [22,23].

Usually, large amount of water transports at the beginning of the channel where electro-osmosis dominates over back diffusion [1]. As a result, anode becomes dried out and the proton conductivity decreases. In that circumstance, the external humidification of the anode and cathode channels enhances the performance of the fuel cell [1–3]. It is also emphasized that higher humidification temperature increases the cell performance and keeps the membrane well hydrated [2,3]. During the fuel cell operation, the H^+ ions move from anode to cathode and pull one to five water molecules, which are 'dragged' for each proton [24,25]. At high current density operation, the anode side can become dried out even though the cathode side is well hydrated [26]. Setting higher anode inlet temperature (with humidified conditions) ensures that membrane will not dry out (at least). Nguyen and White [2] reported that the temperature difference should be 10–15 °C between humidification temperature and the cell temperature. Recently, Lee et al. [27] and Shimpalee et al. [28] reported from their experimental investigations that the optimum cell performance could be achieved for higher anode humidification inlet temperature. A three-dimensional model was developed by Dutta et al. [4,5] with humidification conditions, and net water transport across the MEA (membrane electrode assembly) was investigated. The water vapor in the cell also converts into liquid water depending on saturation

pressure. Condensation of humidified anode and cathode streams are also major issue to keep the MEA well hydrated. Shimpalee and Dutta [6] extended the works of Dutta et al. [4] including phase transformation and energy equation. Indeed, the liquid water in the cell congests the pores of membrane and GDL (Gas Diffusion Layer), and lessens the consumption of reactants. In fact, humidified reactants for both anode and cathode cause some extra cost, weight and complexity of the system [26]. Reactants flow behavior and water management for different current densities along with thermal management for different anode and cathode humidified conditions need to be investigated in detail in a complete three-dimensional model.

There are very few researches focused on reactants flow distribution along and across the channels and the cell performance. At the entrance of the cell membrane conductivity is higher and it causes higher rate of consumption of the reactants. With the increase of current densities the reactants are depleted at the downstream of the channels, which causes the concentration losses [7,8]. Depending on current densities the cell temperature varies. Depending on the cell temperature water vapor and liquid water form in the cell, which creates the problems with flooding or concentration losses. Reactants flow and temperature distributions in the cell were reported by Nguyen et al. [9], Um et al. [10,11] and Lum and McGuirk [12] for specific current density, different dilution and humidification conditions. These models were extended to three-dimensional and for different flow field patterns. However, their model was for isothermal cases and did not consider the phase transformation between water vapor and liquid water.

Recently, Hwang et al. [13], Weng et al. [14] and Su et al. [15] have conducted researches on water transportation and concentration distribution for different parallel and integrated flow fields. These recent results showed that there are non-uniform distributions of H_2 and O_2 at their respective channels for high current densities, which reduces the overall performance of the cell. Water vapor and liquid water in both channels directly control the reactants consumption and their flow distributions. The total process is significantly dominated by current densities and the cell temperature. It is also reported by Weng et al. [14] that without humidification of hydrogen and oxygen causes lower membrane conductivity and current density and the cell performance could be unstable for low humidity and high operating current density conditions. It is important to know the details of reactants and water distribution in the cell for different operating conditions in the cell with proper water and thermal management with a complete three-dimensional, non-isothermal and phase transformation between water vapor and liquid. In this paper, we intend to compute a three-dimensional single straight channel model for fully humidified conditions to investigate the reactants, water vapor and liquid water flow behavior, temperature distribution and water transportation for PEMFC for different current densities and also for different anode and cathode humidified conditions.

The objective of the present study is to investigate the local flow behaviors of the reactants along channels and across the cell and their effects on the total water management process in PEMFC. The investigation has been extended for low, medium and moderate high and high current densities. A three-dimensional model has been chosen with a single straight channel geometry for the numerical simulations. Local flow behaviors of the reactants along the channel and across the cell and their effects on local water transportation across the membrane have been discussed for different current densities. Moreover, the water vapor and liquid water formation and mole fraction along the channels for both anode and cathode have been explained. The temperature, local current density with thermal management, net water transportation and velocity distributions in the cell have been analyzed in detail for the overall performance of the cell. We also intend to investigate detail water and thermal management and reactants and velocity distributions for different anode and cathode humidified conditions. The simulation results have been validated against the available literature results.

2. Numerical simulation

A schematic diagram of the computational domain and its cross-sectional view is shown in Fig. 1. The simple geometry consists of two channels (for hydrogen and air) and the channels sandwich the MEA. There are bipolar plates on both anode and cathode sides where the plates work as a current collector. Humidified hydrogen and air are introduced in the respective channel depending on the stoichiometric rate. The flow is considered as laminar and steady state flow. The governing equations for numerical simulation are: conservation of mass, momentum transport, species transport and energy equations.

Conservation of mass equation

$$\nabla \cdot (\rho \vec{u}) = S_{\mathrm{m}}. \tag{1}$$

The source terms are

$$S_{\mathrm{m}} = S_{\mathrm{H_2}} + S_{\mathrm{wv}_p} + S_{\mathrm{wl}_p} + S_{\mathrm{awv}_e}, \tag{1.1}$$

$$S_{\mathrm{m}} = S_{\mathrm{O_2}} + S_{\mathrm{wv}_p} + S_{\mathrm{wl}_p} + S_{\mathrm{cwv}_e}, \tag{1.2}$$

$$\text{where} \quad S_{\mathrm{H_2}} = -\frac{M_{\mathrm{H_2}} A_{\mathrm{cv}} I}{2F}, \quad \text{and} \quad S_{\mathrm{O_2}} = -\frac{M_{\mathrm{O_2}} A_{\mathrm{cv}} I}{4F}. \tag{1.3}$$

The water vapor at anode and cathode sides is

$$S_{\mathrm{awv}_e} = -\frac{M_{\mathrm{H_2O}} A_{\mathrm{cv}} \alpha I}{F}, \tag{1.4}$$

$$S_{\mathrm{cwv}_e} = S_{\mathrm{cwv}_t} + S_{\mathrm{cwv}_p} = \frac{M_{\mathrm{H_2O}} A_{\mathrm{cv}} I}{2F} + \frac{\alpha M_{\mathrm{H_2O}} A_{\mathrm{cv}} I}{F} = \frac{(1+2\alpha) M_{\mathrm{H_2O}} A_{\mathrm{cv}} I}{2F}. \tag{1.5}$$

The change of phases between water vapor and liquid water depends on partial pressure and is defined as

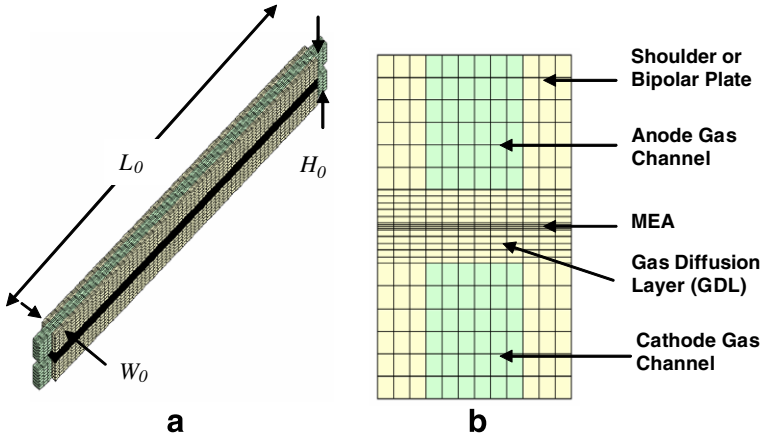

Fig. 1. Single straight channel flow field for PEMFC: (a) geometry, (b) cross-sectional view.

$$S_{\mathrm{wl}_p} = -S_{\mathrm{wv}_p} = -\frac{M_{\mathrm{H_2O}} \sum_{n \text{ of } v} \frac{\mathrm{mass}_{n \text{ of } v}}{M_{n \text{ of } v}}}{\left(1 - \frac{P_{\mathrm{wv}}^{\mathrm{sat}}}{P}\right)} \left[\frac{P_{\mathrm{wv}}^{\mathrm{sat}} - P_{\mathrm{wv}}}{P}\right] * r. \tag{1.6}$$

α in Eqs. (1.3)–(1.5) is the net water transfer coefficient per proton

$$\alpha = n_{\mathrm{d}} - \frac{FD_{\mathrm{W}}[C_{\mathrm{wc}} - C_{\mathrm{wa}}]}{It_{\mathrm{m}}}. \tag{1.7}$$

The electro-osmotic drag coefficient (n_{d}) and water diffusion coefficient (D_{W}) can be correlated with membrane water content (λ) [29]

$$n_{\mathrm{d}} = 0.0029\lambda^2 + 0.05\lambda - 3.4 \times 10^{-19}. \tag{1.8}$$

Momentum transport equation

$$\nabla \cdot (\rho \vec{u}\vec{u}) = -\nabla P + \nabla \cdot (\mu \nabla \vec{u}) + S_{\mathrm{p},i}. \tag{2}$$

where $S_{\mathrm{p},i}$ is the sink source term for porous media in x-, y- and z-directions

$$S_{\mathrm{p},i} = -\left(\sum_{j=1}^{3} \frac{1}{\beta_j} \mu u_j\right). \tag{2.1}$$

Here β is the permeability.

General species transport equation

$$\nabla \cdot (\rho m_n \vec{u}) = \nabla \cdot (J_n) + S_{\mathrm{s}}. \tag{3}$$

Here 'n' denotes for H_2, O_2, water vapor and liquid water. The source terms are the same as those of the conservation of mass equation. The diffusion mass flux (J) of species n in ξ-direction is

$$J_{\xi,n} = -\rho D_{\xi,n} \frac{\partial m_{K,n}}{\partial \xi}, \tag{3.1}$$

where ξ is the dummy variable for direction x, y or z.

Energy equation

$$\nabla(\rho \vec{u} h) = \nabla \cdot (k \nabla T) + S_h. \tag{4}$$

The source term S_h can be obtained by energy losses and heat source by phase change. The heat source from the electrochemical reaction

$$S_{h_e} = h_{\mathrm{rxn}} \left[\frac{IA_{\mathrm{cv}}}{2F}\right] - IV_{\mathrm{cell}} A_{\mathrm{cv}}. \tag{4.1}$$

This electrochemical heat source is given by the difference of the total energy released by the electrochemical reaction at the cathode membrane surface and the electrical energy extracted out of the fuel cell [30]. The heat source by phase change

$$S_{h_p} = S_{\mathrm{wl}_p} * h_{\mathrm{fg}}, \tag{4.2}$$

where h_{fg} is the enthalpy of formation of water. The local current density of the cell is calculated from the open circuit voltage (V_{oc}) and the losses

$$I = \frac{\sigma_{\mathrm{m}}}{t_{\mathrm{m}}} \{V_{\mathrm{oc}} - V_{\mathrm{cell}} - \eta\}, \tag{5}$$

where t_{m} is the membrane thickness and σ_{m} is the membrane conductivity and defined as

$$\sigma_{\mathrm{m}} = \left(0.514 \frac{M_{\mathrm{m,dry}}}{\rho_{\mathrm{m,dry}}} C_{\mathrm{wa}} - 0.326\right) \cdot \exp\left(1268\left(\frac{1}{T_0} - \frac{1}{T}\right)\right), \tag{6}$$

where $T_0 = 303$ K. The local overpotential for the PEMFC can be written as

$$\eta = \frac{RT}{\alpha_{\mathrm{c}} F} \ln\left[\frac{IP}{I_{0_{\mathrm{O_2}}} P_{0_{\mathrm{O_2}}}}\right] + \frac{RT}{\alpha_{\mathrm{a}} F} \ln\left[\frac{IP}{I_{0_{\mathrm{H_2}}} P_{0_{\mathrm{H_2}}}}\right], \tag{7}$$

where P is the pressure and P_0 is the partial pressure of the reactants. α_{a} and α_{c} are the transfer coefficients for anode and cathode respectively. The above all governing equations and appropriate boundary conditions were solved by using the user coding capabilities of STAR-CD that employ a finite volume method. The geometrical and physical parameters for these studies are shown in Tables 1 and 2, respectively.

Table 1
Geometrical parameters

Parameters	Value (mm)
Channel length	34.7
Channel width	1
Channel height	1
Membrane Length	31.7
Membrane thickness	0.05
Anode gas diffusion layer	0.25
Cathode gas diffusion layer	0.25

Table 2
Physical and electrochemical parameters

Parameters	Value	Value (Dutta et al. [4])
Anode pressure (atm)	1	1
Cathode pressure (atm)	1	1
Stoichiometric rate at anode	1.2	2.0
Stoichiometric rate at cathode	2.0	2.0
Cell temperature (°C)	70	70
Anode inlet temperature (°C)	80	80
Cathode inlet temperature (°C)	70	80
Open circuit voltage (V)	0.96	1.1
Relative humidity at anode (%)	100	100
Relative humidity at cathode (%)	100	0
Oxygen inlet mole fraction	0.143	1.0
Oxygen exchange current density (A/m^2)	200	100
Hydrogen exchange current density (A/m^2)	2000	1000
Anode transfer coefficient	1.2	1.0
Cathode transfer coefficient	0.6	0.5
Porosity	0.7	0.7
Permeability (m^2)	1×10^{-12}	2×10^{-10}

3. Results and discussion

Before proceeding further, it is important to establish the reliability of our simulation results. To achieve this, we chose the physical parameters (Table 2) used by Dutta et al. [4] and obtained the polarization curve for our single straight channel geometry and compared with our present results. The comparison of these two polarization curves is shown in Fig. 2. The trend of these two polarization curves is similar, however, there is almost a constant voltage difference between these two curves due to the some differences in physical parameters, i.e., open circuit voltage, exchange current density, transfer coefficient, permeability, reactants inlet boundary conditions, and so forth (Table 2). In general, as it is expected, the cell voltage drops sharply at low current density due to the activation losses. At the middle range of the current densities, the cell voltage drops due to the ohmic losses. For high current densities, the voltage plummets again because of the concentration losses. In the first part of this present study, four different average current densities 0.1 (*low*), 0.6 (*medium*), 1.0 (*moderate high*) and 2.4 (*high*) A/cm^2 for fully humidified (both anode and cathode) conditions have been chosen and discussed on different fluid dynamic aspects and electrochemical issues in the following sections.

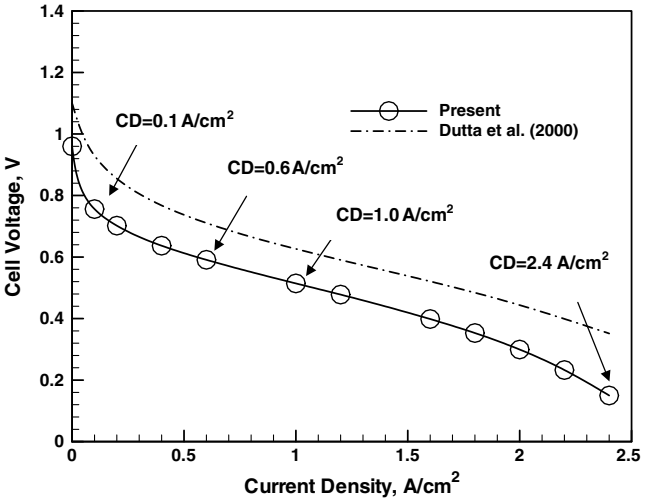

Fig. 2. Polarization curve.

Hydrogen and oxygen consumptions in PEMFC depend on the current density, membrane conductivity and also on the total water management. The reactants mole fractions along the channel length at the channel–GDL interface are shown in Fig. 3. For low to moderate high current densities ($I_{avg} = 0.1$–1.0 A/cm^2), hydrogen mole fraction increases in the anode channel to a certain length with increasing current density and then decreases to the exit of the channel (Fig. 3a). However, for higher current density ($I_{avg} = 2.4$ A/cm^2), hydrogen mole fraction does not show the same trend. In fact, hydrogen mole fraction decreases monotonically along the channel to the exit. On the contrary, for all current densities, oxygen mole fraction decreases all the way of the channel length to the exit (Fig. 3b). There are some inconsistency at the inlet and outlet region, this is because the GDL and membrane length is

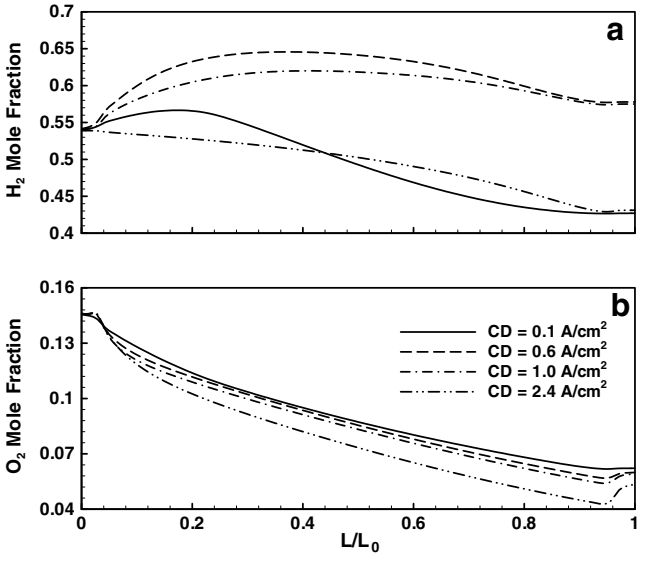

Fig. 3. Height average mole fraction along the channel at $W/W_0 = 0.5$: (a) hydrogen, (b) oxygen.

shorter at both inlet and outlet by 1.49 mm (the membrane length is $L/L_0 = 0.043$ to $L/L_0 = 0.957$). Similar trend of oxygen profile along the length was found by Garau et al. [7], Um et al. [10,11], Lum and McGuirk [12] and Pasaogullari and Wang [31]. This significant behavior of hydrogen mole fraction (Fig. 3a) for different current densities is attributed to many aspects especially on water management process in PEMFC.

In this present study, fully humidified (100%) hydrogen and air are introduced in the anode and cathode channels respectively (see Table 2). Usually, each H^+ ion drags more than one water molecule from anode to cathode due to the electro-osmosis. The consequence of this shows that water vapor mole fraction ($H_2O_{v,a}$) decreases in the anode channel (Fig. 4a). Condensation is another reason of decreasing water vapor mole fraction faster at the initial zone. As the anode inlet temperature is set 80 °C, which is 10 °C higher than the cell temperature, this enforces the water vapor to condense to liquid water. This is evident that the liquid water mole fraction ($H_2O_{l,a}$) increases faster for low current densities especially at 0.1 A/cm^2 (Fig. 4b). Near the inlet region of the cell, the membrane is well hydrated which leads to have higher conductivity and higher electro-osmotic drag coefficient [1,2]. At the downstream of the channels, the water content at the cathode channel dominates over electro-osmosis and also reduces the net water flux.

At the cathode channel, both water vapor ($H_2O_{v,c}$) and liquid water ($H_2O_{l,c}$) mole fraction increase along the cathode channel for all current densities. However, water vapor increases faster for high current densities (see Fig. 5a) and liquid water increases faster for low current densities (see Fig. 5b). In fact, in the cathode stream the total water vapor content increases in different ways – (a) electro-osmosis, where H^+ ions drag water molecules from anode

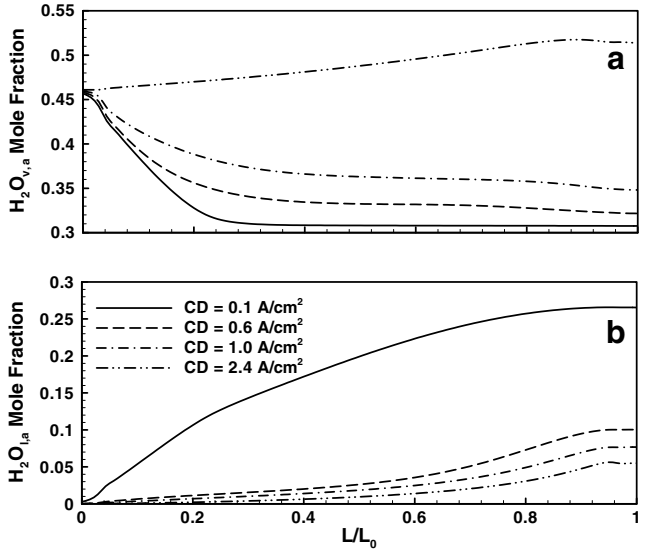

Fig. 4. Height average mole fraction along the anode channel at $W/W_0 = 0.5$: (a) water vapor; (b) liquid water.

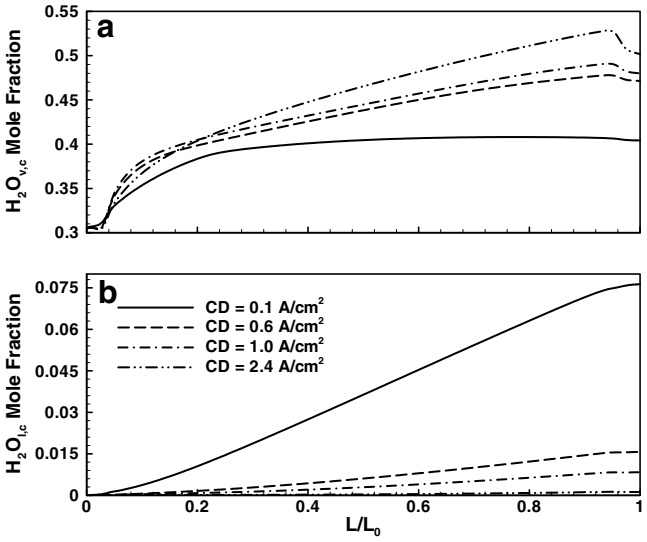

Fig. 5. Height average mole fraction along the cathode channel at $W/W_0 = 0.5$: (a) water vapor; (b) liquid water.

and membrane to the cathode channel, (b) diffusion, i.e., the concentration gradient, and (c) oxygen reduction reaction (ORR), where the byproduct is water. At low current densities the cell temperature is comparatively low (see Fig. 7) and insists the water vapor to condense to liquid water. This causes water vapor to condense and increases liquid water content in the cathode channel faster for low current densities. With the increase of current densities, condensation tendency diminishes due to higher cell temperature.

Before going further once again, we focus on hydrogen mole fraction behavior along the channel, where hydrogen mole fraction increases near the anode inlet region. In order to explain further, we have calculated the reactants mole flow rate along the anode channel at channel–GDL interface. The calculated mole flow rates of hydrogen, water vapor and liquid water at the anode channel for low and high current densities are shown in Fig. 6. It is evident that hydrogen is consuming at GDL and gradually depleting along the channel. However, for low current density, the mole flow rates of hydrogen and water vapor decrease faster near the inlet region because of high membrane conductivity. The mole flow rates of hydrogen and water vapor decrease monotonically along the channel for high current density (see Fig. 6b).

The water (vapor and liquid) distributions along the channels in both anode and cathode (Figs. 4 and 5) indicate that the current density has significant influences on total water management in PEMFC. The flow distribution of the reactants and water at both anode and cathode insists us to examine further thermal and water management in PEMFC. Temperature distributions through the membrane (z-direction) at $L/L_0 = 0.5$ for different current density ranges are shown in Fig. 7. Note that the maximum temperature of the cell is at the membrane, however, the cathode channel–GDL interface exhibits higher tempera-

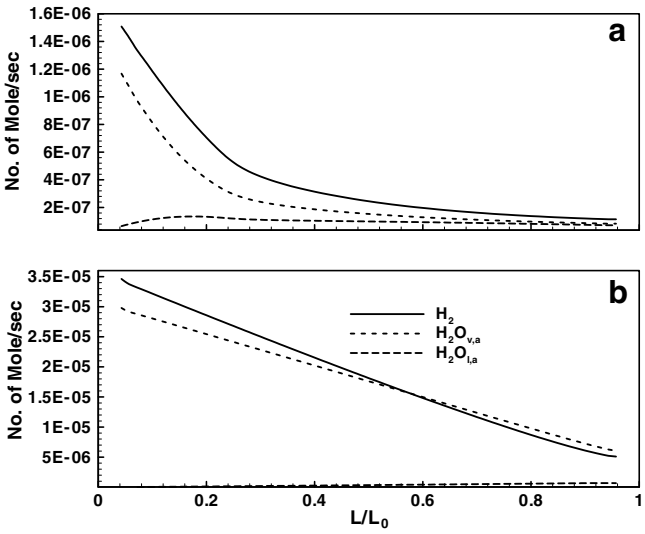

Fig. 6. Mole flow rate along the channel at anode channel–GDL interface and $W/W_0 = 0.5$: (a) current density 0.1 A/cm^2; (b) current density 2.4 A/cm^2.

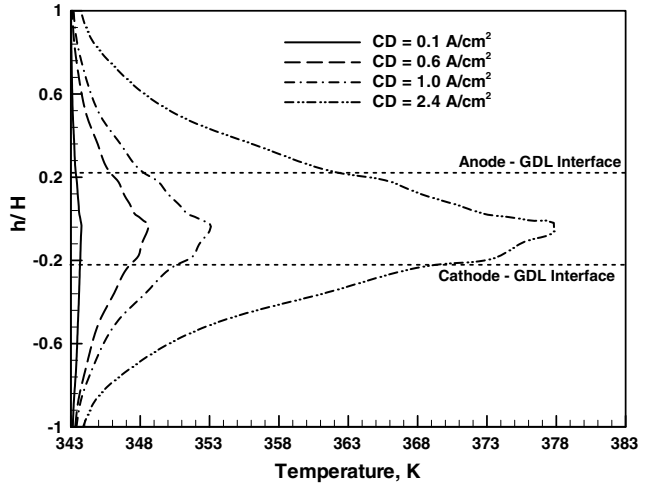

Fig. 7. Temperature profile through the membrane at $L/L_0 = 0.5$ and $W/W_0 = 0.5$.

ture than anode channel–GDL interface because of the exothermic nature of the chemical reaction. Recently, Ju et al. [32] has also found the similar trend of temperature distribution through the membrane of the cell. This higher temperature at the cathode channel–GDL interface increases the water vapor saturation pressure and reduces the tendency to condense the water vapor. Eventually, no liquid water exhibits in the cathode channel at high current density. On the other hand, at the anode channel there is some liquid water at the downstream of the anode channel. This can be explained through the following paragraphs.

Continuing the thermal analysis of this single straight channel flow field, we calculated the temperature along the channel at channel–GDL interface (see Fig. 8). Note that the membrane and GDL length is $L/L_0 = 0.043$ to $L/L_0 = 0.957$. At the initial region of anode channel, the

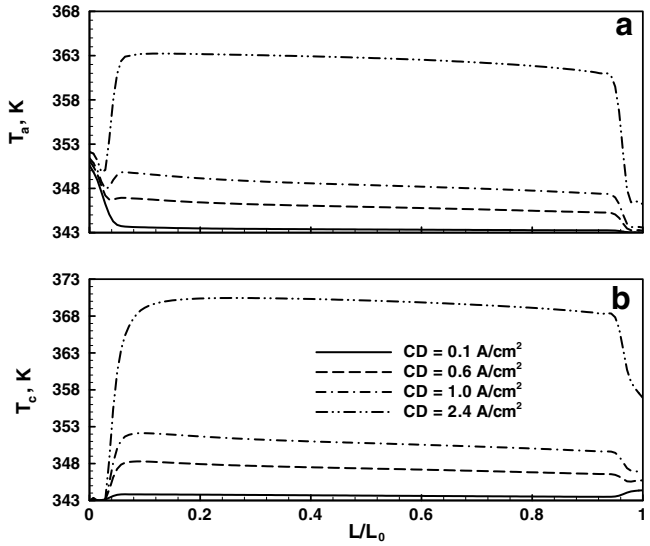

Fig. 8. Temperature distribution along the channel at channel–GDL interface and $W/W_0 = 0.5$: (a) anode, (b) cathode.

temperature decreases up to the length around $L/L_0 = 0.043$ as the inlet temperature is 10 °C higher than the cell temperature. For low current densities the temperature decreases steadily till the exit, however, for high current densities the temperature increases sharply (just after $L/L_0 = 0.043$) and gradually decreases to the exit. In the case of cathode side, cathode channel–GDL interface temperature remains constant up to $L/L_0 = 0.043$ and increases sharply after that and gradually decreases to the exit for all current densities. Similar trend of temperature distribution was also found by Fuller and Newman [1] and Dannenberg et al. [3]. The sharp increases of temperature at the initial zone of the channels emphasize that the water evaporates from the membrane and decreases the membrane conductivity (Fig. 9a). However, at the down-

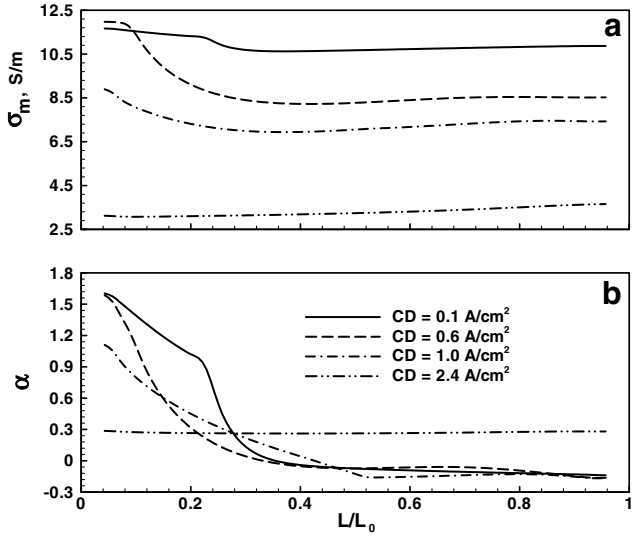

Fig. 9. (a) Membrane conductivity, (b) net water flux per proton at membrane-anode GDL interface, $W/W_0 = 0.5$.

stream of the channels the slow temperature decrease indicates that there is some condensation of water vapor to liquid water. Moreover, water content in the membrane increases through the back diffusion (Fig. 9b) and increases the membrane conductivity (Fig. 9a). This is one of the reasons that little amount of water exhibits at the downstream of the anode channel (Fig. 4a).

This temperature distribution along the channel and through the membrane of the cell (Figs. 7 and 8) directly stimulates the water management of PEMFC. It is clear from Fig. 9a that the membrane conductivity (σ_m) decreases for higher current density. In addition to this, the membrane conductivity (for particular current density) gradually decreases along the length to some distance and increases again for the rest of the membrane/channel length. Fig. 9b shows the net water flux per proton for different current densities. For low range current densities ($I_{avg} =$ 0.1–1.0 A/cm^2), the electro-osmosis is higher at the initial region of the channel. However, the back diffusion takes place in the system and starts to dominate gradually over electro-osmosis rest of the channel length. Higher cell temperature at this high current density plays a significant role on water management in PEMFC. In general, at high current density the hydrogen and oxygen consumption is higher and the water content in the anode channel increases faster (Fig. 4a) due to the anode humidification and low membrane conductivity. This higher amount of water vapor resists the back diffusion and keeps almost constant net water flux per proton through out the length.

The dimensionless local current density (at the membrane–cathode GDL interface) distribution along the length and across the cell (y-direction) is shown in Fig. 10. At low current density I/I_{avg} lessens faster along the length (Fig. 10a), however, current density exceeds the average value near the inlet region and decreases to below the average value at the outlet. At high current density ($I_{avg} = 2.4$ A/cm^2), the local current density does not reach the average value. In contrast, the current density (membrane–GDL interface) distribution along the width indicates that the local current density is higher at the channel area and decreases at the shoulder area for low current density (see Fig. 10b). However, with the increasing of average current density, the local current density decreases in the channel area and gradually increases at the shoulder area (at $L/L_0 = 0.5$). The MEA becomes dehydrated with increasing the current density and usually water reaches the MEA through the gas channels and shoulders. When water flow reaches the MEA from gas channels, current density at the gas channel centerline is higher. When water flow reaches the MEA through the shoulder, the current density at the shoulder is higher than the gas channel [4]. Both nature of local current density can be found along the channels depending on the water transportation to the MEA. Here the water (vapor and liquid) mole fractions across the cell (y-direction) at $L/L_0 = 0.5$ are illustrated in Fig. 11 for the average current density 2.4 A/cm^2. It is evident that liquid water (Fig. 11b) is accumulating at the shoulder region both at anode and cathode compared with the channel area at this particular position ($L/L_0 = 0.5$). Fig. 11a shows that water vapor at anode is almost constant along the width but in the cathode channel water vapor is accumulating in the shoulder area. Indeed, higher amount of water at the shoulder leads to have higher local current density at the shoulder region. However, too much water in the shoulder area congests the pores of the GDL and arises the problems with scarcity of the reactants. In these circumstances local current density also decreases in

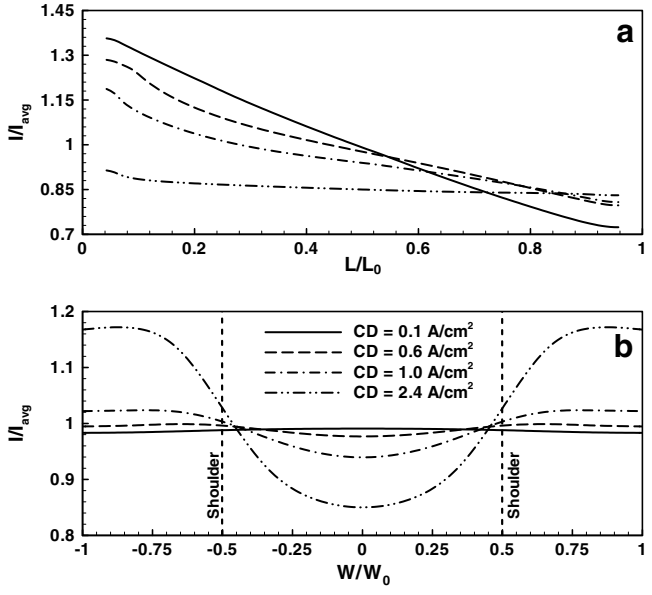

Fig. 10. Non-dimensionalised local current density profile at membrane–cathode GDL interface (a) along the length at $W/W_0 = 0.5$ and (b) along the width at $L/L_0 = 0.5$.

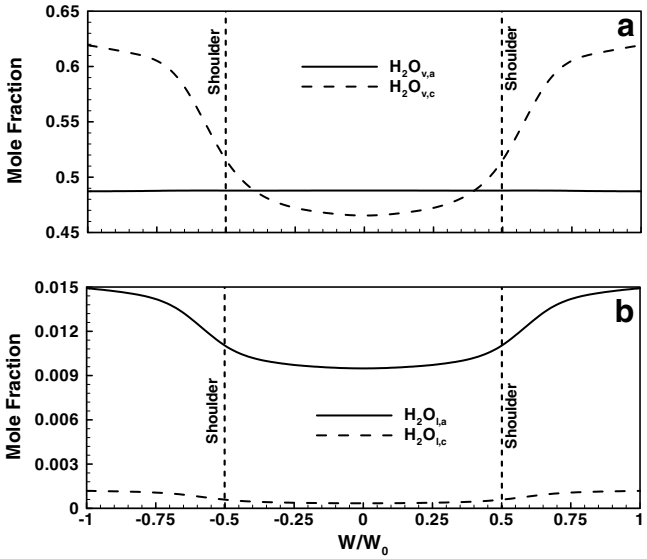

Fig. 11. Mole fraction of water at channel–GDL interface and $L/L_0 = 0.5$ position for current density 2.4 A/cm^2: (a) water vapor, (b) liquid water.

the shoulder area [33]. This significant behavior also depends on the electronic conductivity of the membrane, GDL thickness and gas channel width [34].

Velocity profile also influences the diffusion of the reactants and water vapor to the MEA. Here the velocity profiles at different axial position for both anode and cathode are shown in Fig. 12 for the current density ($I_{avg} = 0.1$ A/cm^2). The velocities both at anode and cathode are non-dimensionalized by their respective inlet velocities. The velocity at the anode channel gradually decreases, however, velocity increases at the cathode channel. It has already been mentioned that hydrogen and water vapor move from anode to cathode through electro-osmosis. This means that the total mass flow along the anode channel decreases (Fig. 12a). This significant behavior also reflects on hydrogen mole flow rate along the channel (Fig. 6). In addition, diffusion also takes place across the membrane depending on the concentration gradient. In the cathode side water is produced due to the chemical reaction with hydrogen and oxygen. These total processes increase the total mass flow in the cathode channel. The effect of increasing the total flow rate results in increasing the velocity along the cathode channel (Fig. 12b). Furthermore, Fig. 13 shows the non-dimensionalized velocity distribution through the membrane of the cell (z-direction) at the anode and cathode sides for different current density operations. Here, the velocities at the anode and cathode sides are also non-dimensionlaized by the respective channel inlet velocities. When the current density is low, the membrane conductivity is higher and as a result much amount of water and hydrogen migrated from anode to cathode. This causes to reduce the velocity in the anode side (as mass flow rate reduced) and causes to increase the velocity in the cathode side as explained above. However, with the increase of operating current densities the membrane conductivity

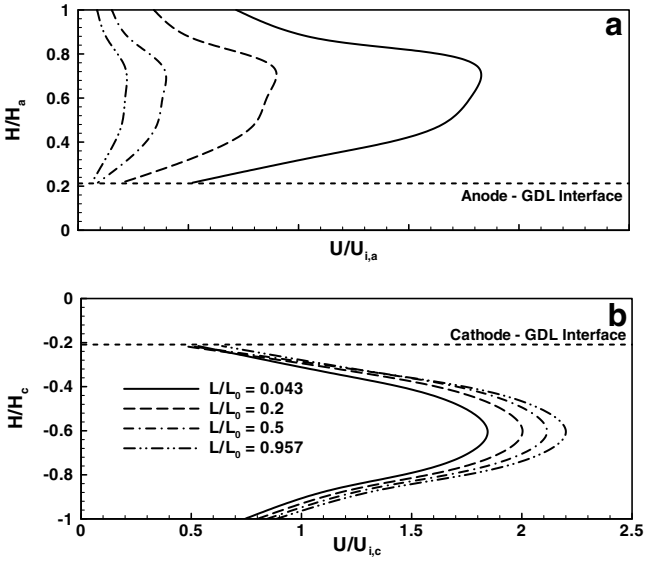

Fig. 12. Velocity profile for current density 0.1 A/cm^2 at $W/W_0 = 0.5$: (a) anode channel, cathode channel.

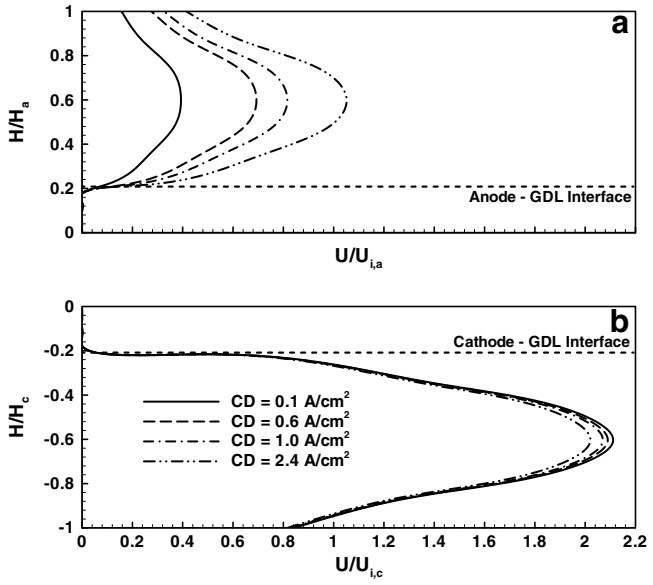

Fig. 13. Velocity profile through the membrane of the cell at $L/L_0 = 0.5$ and $W/W_0 = 0.5$.

decreases. This means that less amount of water and hydrogen migrated from anode to cathode. These ultimately indicate that the rate of change of mass flow rates in the anode channel are getting slower with the increase of current densities. In such circumstances, for a specific zone (e.g., $L/L_0 = 0.5$) the velocity increases in the anode channel for high current densities. On the other hand, in the cathode side the velocity slightly decreased as back diffusion takes place. This velocity distribution indicates that the membrane conductivity is one of the crucial factors of reactants transportation and water management.

To obtain the details of the reactants distribution pattern in fuel cell, we continued our numerical investigations with different anode and cathode humidification conditions. The changing of anode or cathode humidification condition means that the inlet velocity and the reactants and water inlet concentration vary. The general polarization curve for this study is shown in Fig. 14 and clearly indicates that the cell performances are greatly influenced by anode humidification especially at higher current density operations and exhibited poor cell performance for low anode humidified conditions (e.g., A50-C100 means anode and cathode are 50% and 100% humidified respectively). However, low cathode humidified conditions (e.g., A100-C50 or A100-C30) have not reflected such scenario on fuel cell performance. Fig. 15 shows the reactants distributions for two different operating current densities ($I_{avg} = 0.1$ and 1.6 A/cm^2) along the channel length. For low cathode humidified conditions, the hydrogen and oxygen mole fraction show a similar distribution pattern like fully humidified conditions (see Fig. 3) for both low and high operating current densities. On the other hand, for low anode humidified conditions, the hydrogen mole fraction gradually decreases and remain constant (for $I_{avg} =$

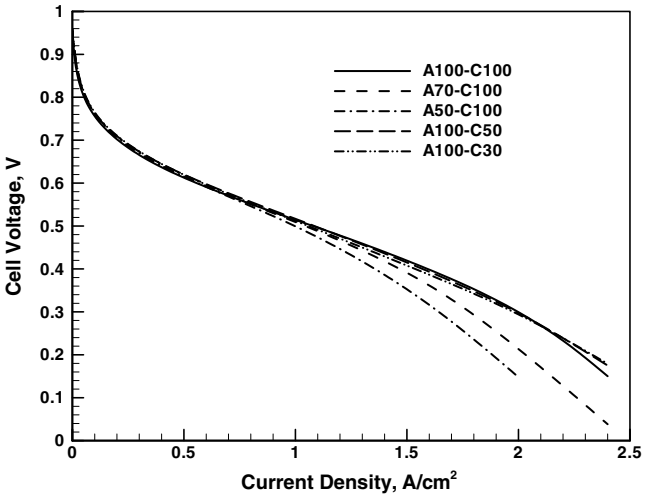

Fig. 14. Cell performance for different humidification conditions.

0.1 A/cm^2) or slowly decreases ($I_{avg} = 1.6$ A/cm^2) till the exit of the channel. This suggests that the reactants distributions are determined by anode humidification conditions where water management plays a crucial part in the fuel cell. However, the complete scenario of reactants distribution could be found in Figs. 16 and 17 which have showed the anode and cathode water distributions, respectively.

In the present model, membrane conductivity depends on anode water activity and as a result, both the electro-osmosis (hydrogen and water migration from anode to cathode) and the back diffusion control the reactants distribution in the cell especially at the anode side. Fig. 18a and b show the membrane conductivity for two different current densities ($I_{avg} = 0.1$ and 1.6 A/cm^2) along the channel length and exhibit a similar pattern on water vapor mole fraction. Fig. 18c and d show the real portrait of water management with net water flux distribution along the channel in the cell for operating current density 0.1 and 1.6 A/cm^2, respectively. With low cathode humidified conditions, electro-osmosis dominates back diffusion especially at the initial region of the channel. However, the back diffusion is going to dominate the electro-osmosis once the anode is considered with low humidified conditions. For operating current density 1.6 A/cm^2 in Fig. 18d, the back diffusion continues to dominate throughout the channel (as the net water flux per proton is close to zero) for different humidified conditions as much more water is produced by chemical reaction. This also causes to increase the membrane conductivity at the downstream of the channel (see Fig. 18b). However, the membrane conductivity is much lower for low anode humidified conditions compared with low cathode humidified conditions. Fig. 19 shows the distribution of different variables for different humidification conditions with operating current density 1.6 A/cm^2. Fig. 19a shows the non-dimensionlaized local current density distribution along the channel width where the local current density is lower at the channel region and higher at shoulder region. It should be noted that the local current density depends on various parameter like membrane conductivity, temperature and different overpotentials [17,33]. The cell temperature slightly increases for low anode humidified conditions especially at the membrane (see Fig. 19b) as the membrane conductivity and water activity are much lower in the system.

Fig. 19c and d show the non-dimensionlaized velocity distribution at the anode and cathode channels for different

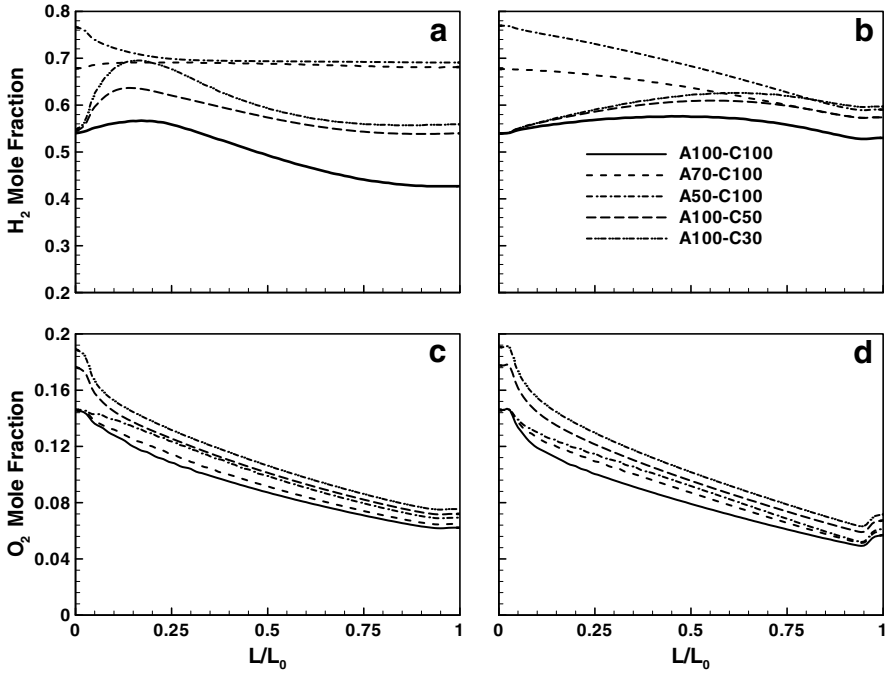

Fig. 15. Mole fraction of hydrogen and oxygen along the channel at $W/W_0 = 0.5$. (a), (c) CD = 0.1 A/cm^2 and (b), (d) CD = 1.6 A/cm^2.

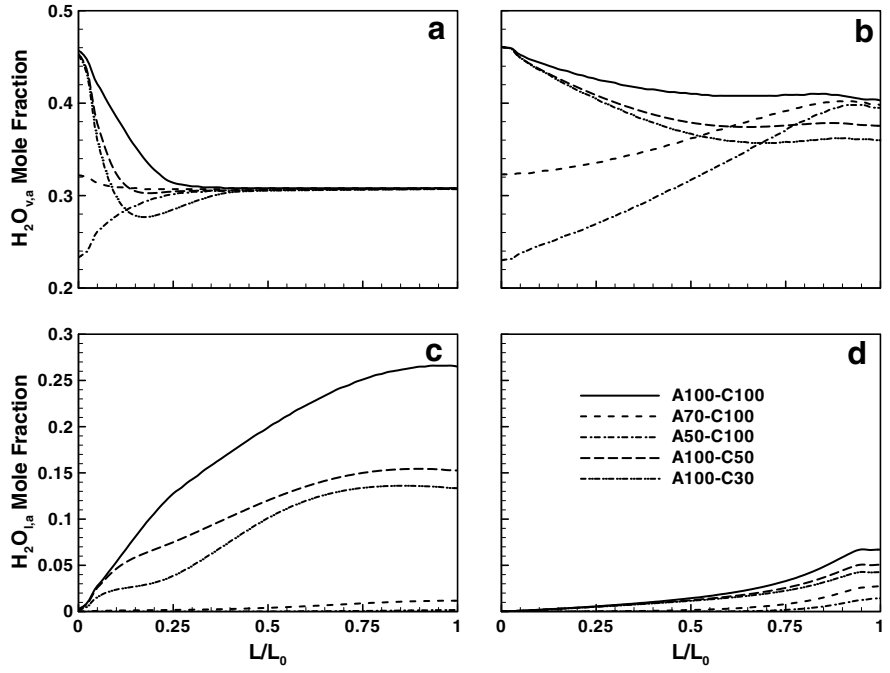

Fig. 16. Mole fraction of water vapor and liquid water at anode side along the channel at $W/W_0 = 0.5$. (a), (c) CD = 0.1 A/cm^2 and (b), (d) CD = 1.6 A/cm^2.

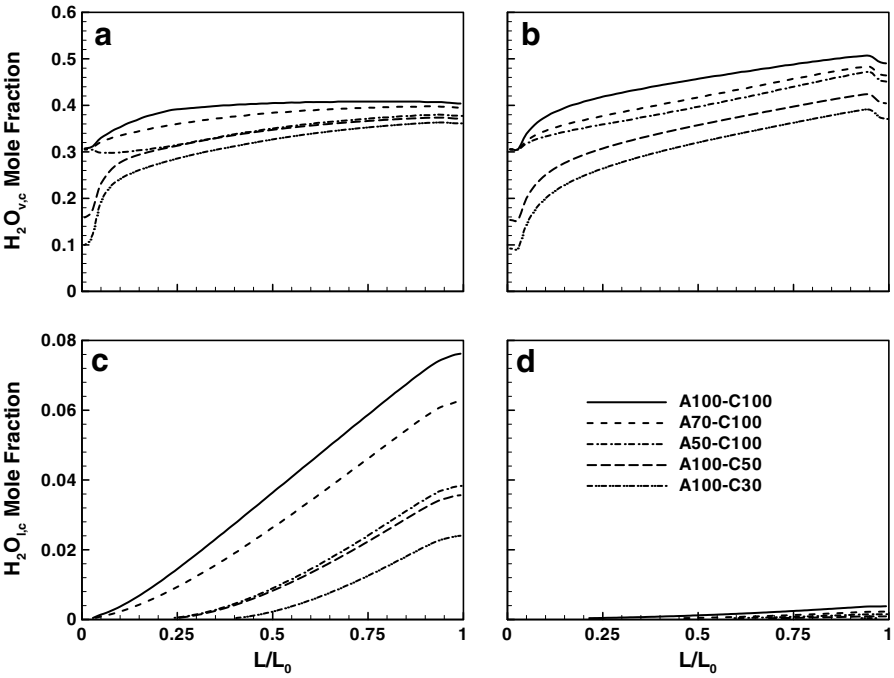

Fig. 17. Mole fraction of water vapor and liquid water at cathode side along the channel at $W/W_0 = 0.5$. (a), (c) CD = 0.1 A/cm^2 and (b), (d) CD = 1.6 A/cm^2.

humidification conditions with operating current density 1.6 A/cm^2 at $L/L_0 = 0.5$ and $W/W_0 = 0.5$. These figures show that when cathode humidification decreases (A100-C100, A100-C50, A100-C30), it causes to increase the velocity in the cathode side as the membrane conductivity is higher due to higher anode humidification. As a result, the velocity in the anode side decreases. On the other hand, when the anode humidification decreases (A100-C100, A70-C100, A50-C100), this causes to decrease the velocity in the cathode side and increases the velocity in the anode side. The velocity variation in the channels can also be attributed to the low membrane conductivity as explained

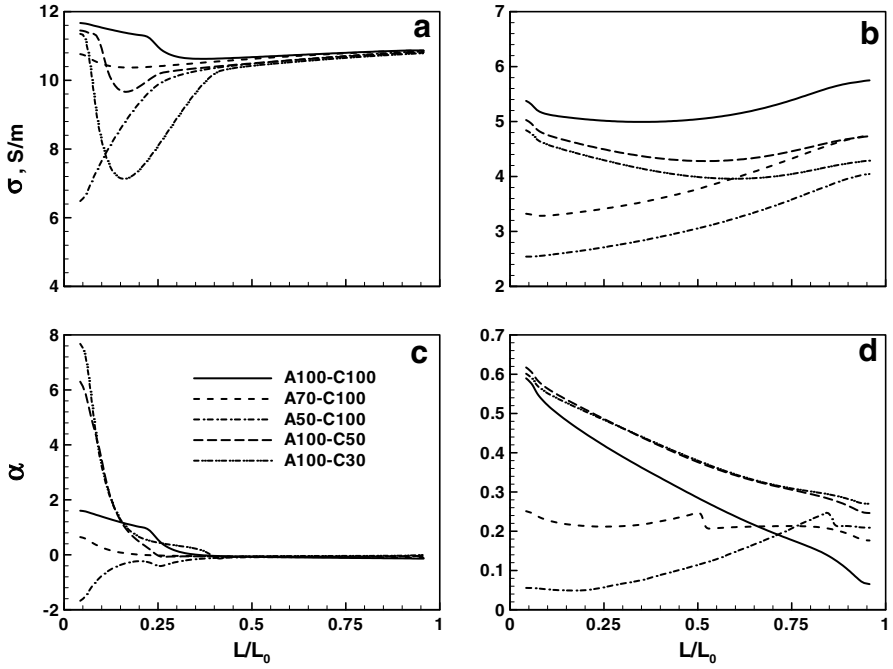

Fig. 18. Variation of membrane conductivity at membrane–anode GDL interface along the length. (a) CD = 0.1 A/cm^2, (b) CD = 1.6 A/cm^2 and net water flux per proton at membrane–cathode GDL interface along the length (c) CD = 0.1 A/cm^2, (d) CD = 1.6 A/cm^2.

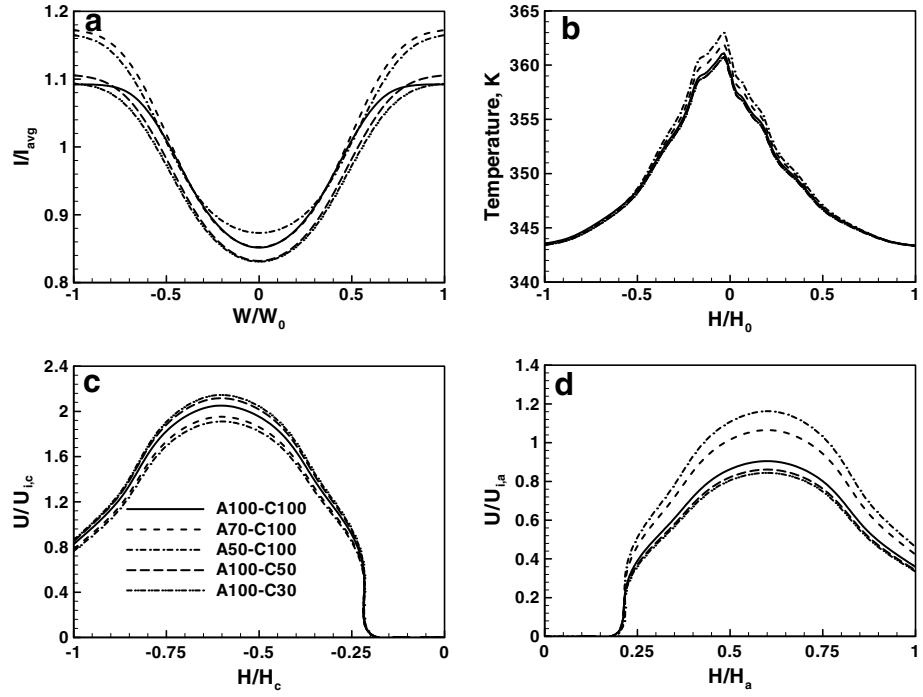

Fig. 19. Variation of different variables for operating current density 1.6 A/cm^2. (a) Non-dimensional local current density along the width at membrane–cathode GDL interface at $L/L_0 = 0.5$ and, (b) temperature distribution through membrane at $L/L_0 = 0.5$ and $W/W_0 = 0.5$, (c) velocity distribution at cathode side and (d) velocity distribution at anode side through membrane at $L/L_0 = 0.5$ and $W/W_0 = 0.5$.

before. The results show that the water management and the reactants' transportation between the channels are also influenced by humidification conditions. The combination of higher anode and lower cathode humidified shows the best performance so far for PEMFC. This combination also shows that the velocity field in the cathode side has

increased which is very essential for the fuel cell to remove the produced water and reduce the flooding in the cell.

4. Summary and conclusions

In the present study, we have carried out the simulations for single straight channel geometry considering different anode and cathode humidification combinations. The main intention of this work was to examine the reactants and water flow behavior in the cell by considering phase transformation among water vapor and liquid water. First, we have investigated the reactants, water vapor and liquid water flow distributions along the channels for different current densities for fully humidified conditions. The simulation results showed that hydrogen mole fraction gradually increased along the channel with increasing current densities. However, hydrogen mole fraction for high current density and oxygen mole fraction for all current density decreased monotonically along the channels. The present model with phase transformation showed that the formation of liquid water at low operating current density was much faster especially at the inlet region of the anode channel. Furthermore, it was found that higher amount of liquid water was accumulated in the shoulder region than in the channel region. In addition, the formation of liquid water decreased significantly for high operating current density as the cell temperature increased. It was revealed from the simulation results that at lower current densities higher amount of water diffused through membrane at the entrance zone of the anode channel because of higher proton conductivity. Moreover, at low current density the anode water vapor condensed faster to liquid water because of low cell temperature. For local current density distribution, near the entrance, the cell had higher local current density and gradually decreased along the length. The water accumulated near the shoulder area rather than in the channels and had higher local current density at the shoulder area. This tendency gradually increased with the increase of current density. We also examined the velocity distribution along and across the cell for different current densities and revealed that the velocity distributions were greatly influenced by membrane conductivity. The present model showed that the current density and cell temperature had significant effects on water management and reactants behavior in PEMFC. We also investigated the reactants distribution and related water management for different humidification conditions and revealed that anode humidification played an important role on water management and also reactants distributions. This present study showed that the combination of higher anode and lower cathode humidification can be helpful for obtaining the best performance of the cell and caused to increase the velocity in the cathode region. Obtaining higher velocity in the cathode channel is very essential for the fuel cell to remove the produced water and reduce the flooding in the cell. In addition, the results showed that the membrane was kept well hydrated and had higher membrane conductivity for higher anode humidification conditions.

Acknowledgement

This work was supported by Korea Research Foundation.

References

[1] T.F. Fuller, J. Newman, Water and thermal management in solid-polymer-electrolyte fuel cells, J. Electrochem. Soc. 140 (5) (1993) 1218–1225.
[2] T.V. Nguyen, R.E. White, A water and heat management model for proton-exchange-membrane fuel cells, J. Electrochem. Soc. 140 (8) (1993) 2178–2186.
[3] K. Dannenberg, P. Ekdunge, G. Lindbergh, Mathematical model of the PEMFC, J. Appl. Electrochem. 30 (2000) 1377–1387.
[4] S. Dutta, S. Shimpalee, J.W. Van Zee, Three-dimensional numerical simulation of straight channel PEM fuel cells, J. Appl. Electrochem. 30 (2000) 135–146.
[5] S. Dutta, S. Shimpalee, J.W. Van Zee, Numerical prediction of mass-exchange between cathode and anode channel in a PEM fuel cell, Int. J. Heat Mass Transfer 44 (2001) 2029–2042.
[6] S. Shimpalee, S. Dutta, Numerical prediction of temperature distribution in PEM fuel cells, Numer. Heat Transfer Part A 38 (2000) 111–128.
[7] V. Gurau, H. Liu, S. Kakac, Two-dimensional model for proton exchange membrane fuel cells, AIChE J. 44 (11) (1998) 2410–2422.
[8] T. Berning, D.M. Lu, N. Djilali, Three-dimensional computational analysis of transport phenomena in a PEM fuel cell, J. Power Sources 106 (2002) 284–294.
[9] P.T. Nguyen, T. Berning, N. Djilali, Computational model of PEM fuel cell with serpentine gas flow channels, J. Power Sources 130 (2004) 149–157.
[10] S. Um, C.Y. Wang, K.S. Chen, Computational fluid dynamics modeling of proton exchange membrane fuel cells, J. Electrochem. Soc. 147 (12) (2000) 4485–4493.
[11] S. Um, C.Y. Wang, Three-dimensional analysis of transport and electrochemical reactions in polymer electrolyte fuel cells, J. Power Sources 125 (2004) 40–51.
[12] K.W. Lum, J.J. McGuirk, Journal of Power Sources formulation, Three-dimensional model of a complete polymer electrolyte membrane fuel cell – model formulation, validation and parametric studies, J. Power Sources 143 (2005) 103–124.
[13] J.J. Hwang, C.K. Chen, R.F. Savinell, C.C. Liu, J. Wainright, A three-dimensional numerical simulation of the transport phenomena in the cathodic side of PEMFC, J. Appl. Electrochem. 34 (2004) 217–224.
[14] F.B. Weng, A. Su, G.B. Jung, Y.C. Chiu, S.H. Chan, Numerical prediction of concentration and current distributions in PEMFC, J. Power Sources 145 (2005) 546–554.
[15] A. Su, Y.C. Chiu, F.B. Weng, The impact of flow field pattern on concentration and performance in PEMFC, Int. J. Energy Res. 29 (2005) 409–425.
[16] S. Shimpalee, W.K. Lee, J.W. Van Zee, H.N. Neshat, Predicting the transient response of a serpentine flow-field PEMFC I. Excess of normal fuel and Air, J. Power Sources 156 (2006) 355–368.
[17] D.H. Ahmed, H.J. Sung, Effects of channel geometrical configuration and shoulder width on PEMFC performance at high current density, J. Power Sources 162 (2006) 327–339.
[18] D. Natarajan, T.V. Nguyen, A two-dimensional, two-phase, multi-component, transient model for the cathode of a proton exchange membrane fuel cell using conventional gas distributors, J. Electrochem. Soc. 148 (12) (2001) A1324–A1335.

[19] H.C. Liu, W.M. Yan, C.Y. Soong, F. Chen, Effects of baffle-blocked flow channel on reactant transport and cell performance of a proton exchange membrane fuel cell, J. Power Sources 142 (2005) 125–133.
[20] H.C. Liu, W.M. Yan, C.Y. Soong, F. Chen, H.S. Chu, Reactant gas transport and cell performance of proton exchange membrane fuel cells with tapered flow field design, J. Power Sources 158 (2006) 78–87.
[21] D.H. Ahmed, H.J. Sung, Design of a deflected membrane electrode assembly for PEMFCs, Int. J. Heat Mass Transfer, in press.
[22] A. Parthasarathy, S. Srinivasan, A.J. Appleby, Pressure dependence of the oxygen reduction reaction at the platinum microelectrode/Nafion interface: electrode kinetics and mass transport, J. Electrochem. Soc. 139 (10) (1992) 2856–2862.
[23] H. Xu, Y. Song, H.R. Kunz, J.M. Fenton, Effect of elevated temperature and reduced relative humidity on ORR kinetics for PEM fuel cells, J. Electrochem. Soc. 152 (9) (2005) A1828–A1836.
[24] T.A. Zawodzinski, C. Derouin, S. Radzinski, R.J. Sherman, V.T. Smith. T.E. Springer, S. Gottesfeld, Water uptake by transport through Nafion 117 membrane, J. Electrochem. Soc. 140 (4) (1993) 1041–1047.
[25] X. Ren, S. Gottesfeld, Electro-osmosis drag of water in a ploy (perfluorosulphonic acid) membrane, J. Electrochem. Soc. 148 (1) (2001) A87–A93.
[26] J. Larminie, A. Dicks, Fuel Cell Systems Explained, second ed., Wiley, England, 2003, pp. 85–90.
[27] W-K. Lee, S. Shimpalee, J.W. Van Zee, Verifying predictions of water and current distributions in a serpentine flow field polymer electrolyte membrane fuel cell, J. Electrochem. Soc. 150 (3) (2003) A341–A348.
[28] S. Shimpalee, S. Greenway, J.W. Van Zee, The impact of channel path length on PEMFC flow-field design, J. Power Sources 160 (2006) 398–406.
[29] T.E. Springer, T.A. Zawodzinski, S. Gottesfeld, Polymer electrolyte fuel cell model, J. Electrochem. Soc. 138 (8) (1991) 2334–2342.
[30] STAR-CD Version 3.24 methodology, CD-Adapco Group.
[31] U. Pasaogullari, C.Y. Wang, Two-phase modeling and flooding prediction of polymer electrolyte fuel cells, J. Electrochem. Soc. 152 (2) (2005) A380–A390.
[32] H. Ju, H. Meng, C.Y. Wang, A single-phase, non-isothermal model for PEM fuel cells, Int. J. Heat Mass Transfer 48 (2005) 1303–1315.
[33] D.H. Ahmed, H.J. Sung, Local current density and water management in PEMFCs, Int. J. Heat Mass Transfer 50 (2007) 3376–3389.
[34] H. Meng, C.Y. Wang, Electron transport in PEFCs, J. Electrochem. Soc. 151 (3) (2004) A358–A367.